Dynamic manipulation of the subharmonic scattering of phospholipid-coated microbubbles

2011 Phys. Med. Biol. 56 6459

(http://iopscience.iop.org/0031-9155/56/19/018)

IOP PUBLISHING PHYSICS IN MEDICINE AND BIOLOGY

Phys. Med. Biol. **56** (2011) 6459–6473 doi:10.1088/0031-9155/56/19/018

Dynamic manipulation of the subharmonic scattering of phospholipid-coated microbubbles

Telli Faez[1,4], Guillaume Renaud[1], Marielle Defontaine[2], Samuel Calle[2] and Nico de Jong[1,3]

[1] Biomedical Engineering Thoraxcenter, Erasmus Medical Center, PO Box 2040, 3000 CA Rotterdam, The Netherlands
[2] INSERM U930-CNRS ERL3106, Université François Rabelais, UFR Médecine, 10 bd Tonnellé, 37000 Tours, France
[3] Physics of Fluids Group, Department of Science and Technology, University of Twente, PO Box 217, 7500 AE Enschede, The Netherlands

E-mail: t.faez@erasmusmc.nl

Received 21 June 2011, in final form 19 August 2011
Published 20 September 2011
Online at stacks.iop.org/PMB/56/6459

Abstract

In this paper, the influence of a dynamic variation in the ambient pressure on the subharmonic response of phospholipid-coated microbubbles was investigated. The ambient pressure in water was modulated by a 2.5 kHz acoustic wave with a peak amplitude of 15 kPa. We investigated the fundamental and subharmonic emissions at two driving frequencies: 5 and 10 MHz. The modulation of the bubble radius induced by the dynamic variation in the liquid ambient pressure subsequently causes modulations of the scattered acoustic pressure at the fundamental and subharmonic frequencies (half the fundamental frequency). As a first result, we measured that the variation in the ambient pressure of 15 kPa can modulate the subharmonic amplitude up to 10 dB as compared to the static atmospheric pressure condition. As a second result, we noticed that the relative subharmonic amplitude modulation as a function of the LF acoustic pressure was symmetrical for the 5 MHz driving frequency but asymmetric for 10 MHz. In the latter case, the subharmonic amplitude was more enhanced for an ambient overpressure than reduced for an ambient depression of the same amplitude likely due to the buckling of the lipid shell. However, the fundamental amplitude was symmetrically modulated during bubble compression and expansion. Moreover, subharmonic and fundamental amplitude modulations were found to be either in phase or out of phase with the low-frequency acoustic pressure. Numerical simulations showed that this behavior can be obtained depending on the bubbles' diameter. The highest subharmonic amplitude was measured when microbubbles were insonified at 10 MHz. This fact together with the asymmetry observed in the subharmonic modulation suggests that smaller bubbles with a buckling shell are excited at

[4] Author to whom any correspondence should be addressed.

10 MHz compared to 5 MHz. These results present new potentials for *in vitro* characterization of contrast agent microbubbles and possibly a new imaging modality.

1. Introduction

Contrast-enhanced ultrasound imaging is a non-invasive technique which has shown great potential in the characterization of the *vasa vasorum* and intra-plaque angiogenesis (Eliasziw *et al* 1995, Baldassarre *et al* 2000, Feinstein 2006, Shah *et al* 2007, Vicenzini *et al* 2007, Coli *et al* 2008, Staub *et al* 2009, Xiong *et al* 2009, Shalhoub *et al* 2010). The goal in utilizing ultrasound (US) contrast agents is to improve the contrast to tissue ratio (CTR) by exploiting the nonlinear acoustical properties of the contrast microbubbles. Therefore, many imaging modalities focus on harmonic imaging such as pulse inversion (Burns *et al* 2000) and power modulation (Brock-Fisher *et al* 1996). Yet, these methods are not optimal because of the nonlinear propagation in tissue and contrast agent (Tang *et al* 2010). Alternatively, a great deal of interest has been put on the use of subharmonic emissions from contrast agents (Shi *et al* 1999, Chomas *et al* 2002). The reason for this interest mainly lies in the fact that tissue does not generate subharmonic energy and subharmonic imaging does not suffer from nonlinear propagation artifacts (Tang *et al* 2010). The feasibility of using subharmonic energy to detect microvascularity has been shown in mice (Goertz *et al* 2005) using Definity™ (Lantheus Medical Imaging, North Billerica, MA, USA) and in rabbit aortas (Goertz *et al* 2007, Needles *et al* 2010). The only human study reported on subharmonic imaging, to the knowledge of the authors, is the detection of breast lesion at a transmit frequency of 4.4 MHz with Optison (GE Healthcare, Chalfont St Giles, UK) contrast agents (Forsberg *et al* 2007). For carotid imaging, higher transmitting frequencies between 5 and 15 MHz are preferred. Optical characterization of contrast agent microbubbles, using a high-speed camera, within the frequency range of interest for carotid imaging (8–12 MHz) has shown the potential of applying this method for vascular imaging (Faez *et al* 2011). The authors show that the subharmonic oscillation of BR14 (Bracco Research SA, Geneva, Switzerland) microbubbles can be generated by low acoustic pressures of order 50 kPa peak amplitude at frequencies around 10 MHz. Their experimental results indicated that 40% of the microbubbles exhibit subharmonic vibrations. These microbubbles may have a very low initial surface tension such that an acoustic overpressure induces buckling of the phospholipid shell. This was supported by numerical calculations based on Marmottant *et al's* (2005) model. Zero surface tension in this model corresponds to bubbles with a buckled shell. These simulations showed that bubbles in the buckling regime generate the highest subharmonic emission (Sijl *et al* 2010, Faez *et al* 2011). So, subharmonic imaging requires engineering bubbles with a buckled shell (zero initial surface tension). To overcome this, we developed a method to manipulate microbubbles such that they exhibit a higher subharmonic response. Frinking *et al* (2010) have shown experimentally and numerically (based on Marmottant *et al's* (2005) model) that the subharmonic amplitude increases when an ambient overpressure is applied to the system for transmit acoustic pressures below 120 kPa. They demonstrate that this can be caused by a change in the value of initial surface tension at equilibrium. The closer the initial surface tension to the buckling state (zero surface tension), the more subharmonic energy is generated. Their experiments show an increase in the subharmonic amplitude up to 20 dB in power by applying an ambient overpressure of around 10 kPa (75 mmHg).

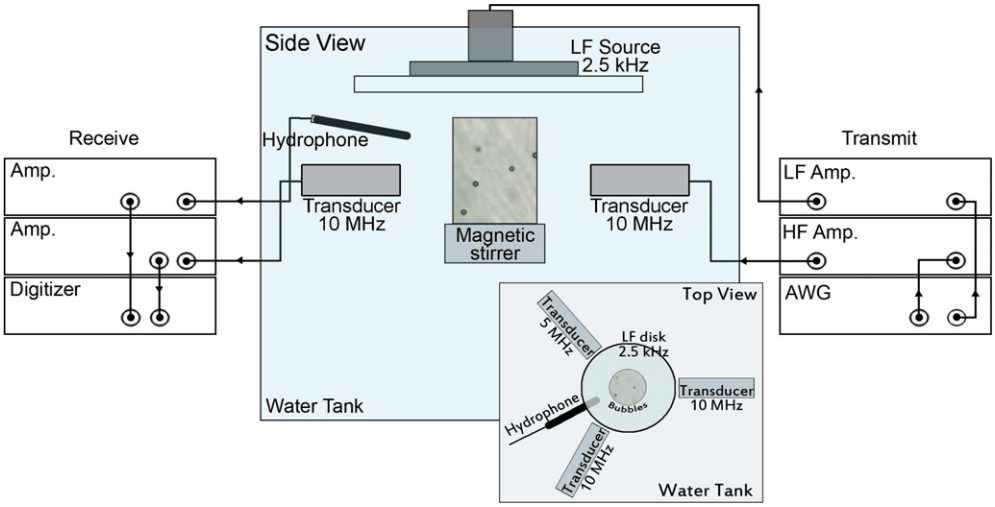

Figure 1. Schematic view of the experimental setup.

In this study, we propose an alternative way to dynamically manipulate the response of the microbubbles by using a very low frequency (LF) wave to change the ambient pressure. We measure and analyze the acoustic scattering of contrast agent microbubbles at the fundamental and subharmonic frequencies for two different driving frequencies of 5 MHz and 10 MHz at a low mechanical index (MI) of 0.07 (156 kPa at 5 MHz and 240 kPa at 10 MHz). The LF acoustic pressure acts as a quasi-static increase and reduction in the ambient pressure. This method is inspired by a similar technique developed to detect micro-cracks in bone tissue (Renaud *et al* 2008, 2009).

2. Materials and methods

2.1. Experimental setup

Figure 1 shows a schematic view of the setup. A sealed container with acoustically transparent walls was filled with a highly diluted (1:15000) suspension of BR14 microbubbles. The bubble container was mounted on a magnetic stirrer to obtain a homogeneous distribution of microbubbles. The center of the container was positioned at the focal distance of the transmitting and receiving US transducers (76 mm). A wideband transducer (V311; 3–13 MHz, Panametrics Inc., Waltham, MA, USA) was used to transmit either 15-cycle 5 MHz or 25-cycle 10 MHz sinusoidal bursts with a repetition rate of 16 kHz and an MI of 0.07. The US echoes scattered by the microbubbles were received by two other focused transducers (V308; 1–7 MHz and V315; 3–13 MHz, Panametrics Inc., Waltham, MA, USA). The transducers were positioned with a 120° angle from each other. The LF acoustic wave was produced by a 15 cm diameter glass disk connected to a shaker, which was excited by a 100-cycle 2.5 kHz sinusoidal burst. Given the LF wavelength and the LF diffraction pattern, the LF wave induced a dynamic modulation of the ambient pressure in the bubble container. A hydrophone (8103, Brüel and Kjær, Nærum, Denmark) was also mounted near the bubble container to measure the pressure wave experienced by microbubbles in the container. The peak amplitude of the LF acoustic wave in the bubble container was 15 kPa. The whole setup

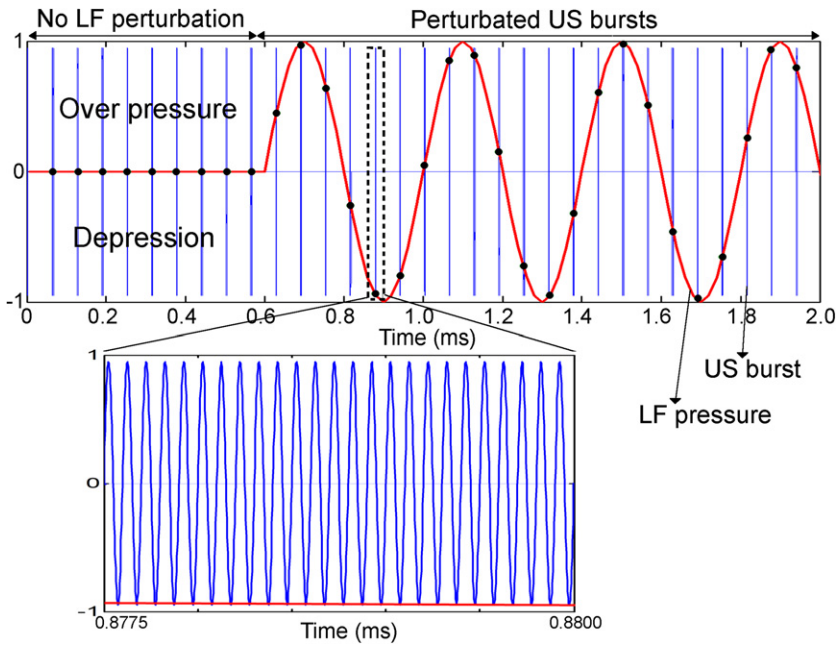

Figure 2. Schematic view of the LF and US signals.

was immersed in water inside a large water tank. The water tank was designed deep enough to prevent significant reflections of the LF wave from the walls of the water tank (Renaud *et al* 2010). Fifty measurements with a 5 MHz transmit frequency and 50 measurements with a 10 MHz transmit frequency were acquired.

2.2. Signal processing

A 50 ms delay was applied in the firing of the LF wave in order to have a reference when comparing the perturbed to the non-perturbed US signals. A 2 ms section of the full signal (with the total duration of 100 ms) is shown in figure 2. The whole US signal contained 1600 US pulses. For the analysis, each received US burst was truncated and its discrete Fourier transform was calculated to retrieve the fundamental (at the transmit frequency) and subharmonic (at half the transmit frequency) amplitudes. Finally, each US burst is associated with the LF pressure value recorded half an US time of flight before the actual time when the US burst is received.

In order to indicate the importance of the variation in the subharmonic and fundamental amplitudes induced by the LF pressure, we estimated the subharmonic and fundamental amplitudes expected without the effect of the LF perturbation by applying a low-pass (LP) filtering (cutoff frequency: 1.1 kHz) on the data. This base line is depicted as a yellow line in figures 3 and 4 where the fundamental and subharmonic amplitudes are presented as functions of the time for transmit frequencies of 5 and 10 MHz. The relative fundamental and subharmonic modulations (RFM and RSM) are defined as the difference between

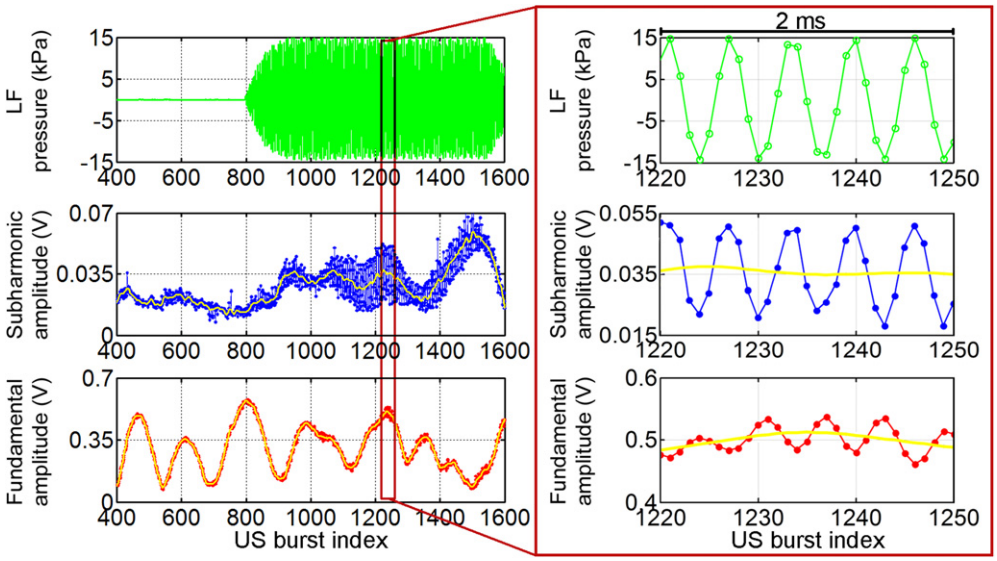

Figure 3. The LF pressure, and the fundamental and the subharmonic amplitudes as functions of the time (US burst index) for transmitting frequency of 5 MHz. The yellow line is obtained by LP filtering and corresponds to the fundamental and the subharmonic amplitudes expected without the effect of the LF perturbation. Each data point is associated with one US burst. The three right panels show a typical time window of 2 ms used for the instantaneous analysis.

the fundamental/subharmonic amplitude and the LP filtered fundamental/subharmonic amplitude, normalized by the LP filtered fundamental/subharmonic amplitude:

$$\text{RFM} = \frac{F - F_0}{F_0} \qquad \begin{cases} F: \text{ fundamental amplitude} \\ F_0: \text{ LP filtered fundamental amplitude} \end{cases}$$
$$\text{RSM} = \frac{S - S_0}{S_0} \qquad \begin{cases} S: \text{ subharmonic amplitude} \\ S_0: \text{ LP filtered subharmonic amplitude.} \end{cases} \tag{1}$$

Thus, the changes in the fundamental and subharmonic amplitudes are expressed relative to their values in the absence of a LF pressure.

3. Results

3.1. Time signals

The recorded LF pressure pulse and measured fundamental and subharmonic amplitudes are presented in figures 3 and 4 for driving frequencies of 5 and 10 MHz, respectively. During the first 50 ms before the firing of the LF wave, no perturbation at 2.5 kHz is observed in the fundamental and subharmonic amplitudes. The slow variation in the fundamental amplitude is due to the passage of single or a cluster of microbubbles in the focal area of the transducers. During the next 50 ms, the scattering properties of contrast agent microbubbles are perturbed by the LF pressure and modulations of the subharmonic and fundamental amplitudes are clearly evident. The zoomed-in region in the right panels of figures 3 and 4 presents an enlarged view of the fundamental and subharmonic modulations around a peak of the fundamental amplitude and during 2 ms, such that the microbubbles are considered quasi-static and located at the focal

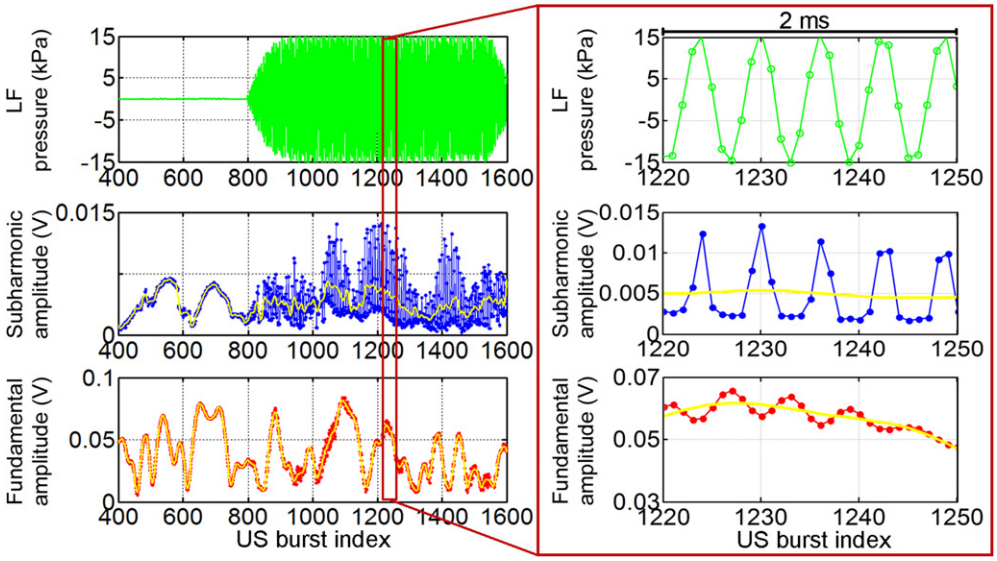

Figure 4. Same caption as figure 3 for a transmitting frequency of 10 MHz.

area of the transducers. This duration equals 5 LF periods and contains 32 high-frequency US bursts. Such time windows are employed for the instantaneous analysis in section 3.2.

For 5 and 10 MHz transmitting frequencies, we observe an increase in the subharmonic amplitude for a positive LF pressure (compression), while for a negative LF pressure (tension) the subharmonic amplitude decreases. However, the subharmonic variation is smaller when microbubbles undergo an expansion (negative LF pressure) than when they are compressed (positive LF pressure) for a transmit frequency of 10 MHz (figure 4). In contrast, the subharmonic modulation is symmetrical for a transmit frequency of 5 MHz (figure 3). As far as the fundamental amplitude is concerned, we observed that for both transmitting frequencies the fundamental variation follows the dynamic changes in the ambient pressure symmetrically, increasing for a negative LF pressure and decreasing for a positive LF pressure.

3.2. Instantaneous analysis

From the whole 100 ms recorded signal, a time window of 2 ms was positioned around each maximum of the fundamental amplitude and during the steady state of the LF pressure signal (US burst index of 1000:1500), to plot the subharmonic and fundamental amplitudes as functions of the LF pressure. In figures 5 and 6, RFM and RSM as functions of the LF pressure for 5 and 10 MHz driving frequencies are shown, respectively. As shown in figures 5 and 6, four typical cases were observed. Case 1 is when RFM and RSM are both in phase with the LF pressure. In cases 2 and 3, either RFM or RSM is out of phase with the LF pressure, and in case 4 both RFM and RSM are out of phase with the LF pressure.

From 50 measurements, roughly 400 peaks were identified in the slow variation in the fundamental amplitude such that around 400 microbubbles were investigated at transmit frequencies of 5 and 10 MHz. Figure 7 indicates the total number of microbubbles analyzed at each driving frequency and a histogram specifying the percentage of microbubbles behaving according to cases 1–4 defined above and presented in figures 5 and 6. For a 5 MHz driving

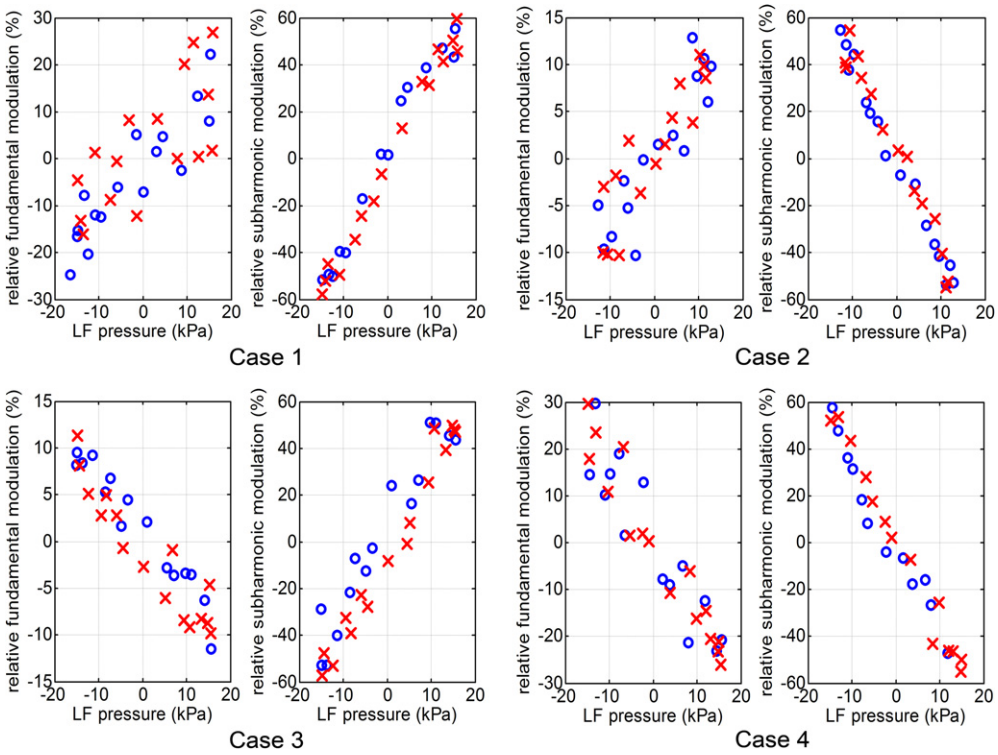

Figure 5. RFM and RSM as functions of the LF pressure for a transmitting frequency of 5 MHz. Circles: increasing LF pressure, crosses: decreasing LF pressure.

frequency, the four cases exhibit a rather equal prevalence between 20% and 35%. In contrast, at 10 MHz transmit frequency 60% of microbubbles follow case 3 and 26% behave like case 1. Cases 2 and 4 are rarely observed with, respectively, 6% and 8%.

4. Discussion

4.1. Effect of ambient pressure change on the fundamental and subharmonic scattering

It was observed that the modulation of the subharmonic and fundamental amplitudes in the signal scattered by microbubbles versus the dynamic change in the ambient pressure can be categorized into four cases; these cases are summarized in table 1. The four mentioned cases were observed for both 5 and 10 MHz transmitting frequencies. However, at 10 MHz, a majority of microbubbles belong to cases 3 and 1. In order to understand the effect of the LF pressure on the scattering properties of US contrast agents, the scattered pressure signal as a function of the bubble diameter for transmitting frequencies of 5 and 10 MHz was calculated based on the models of Marmottant *et al* (2005) and de Jong *et al* (1994).

4.1.1. Numerical simulations based on the Marmottant model (buckling–rupturing shell). Marmottant *et al's* (2005) model was designed to describe the large amplitude response of lipid-coated microbubbles in terms of a varying surface tension. Based on this definition, the bubble dynamics is divided into three regimes: buckled, visco-elastic and ruptured. The

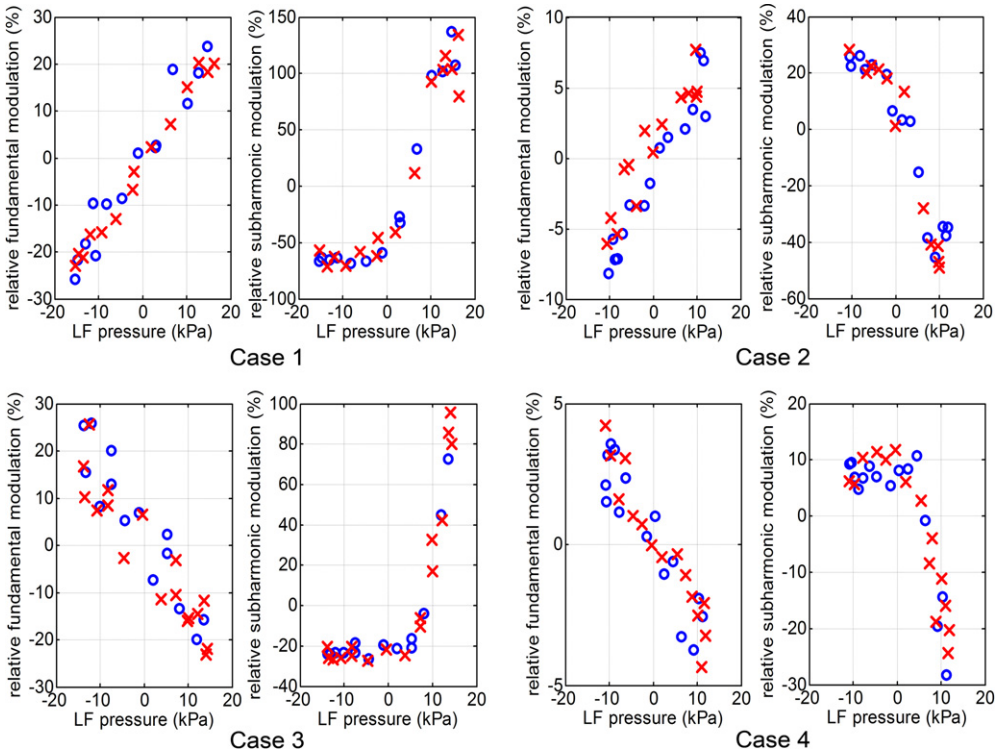

Figure 6. RFM and RSM as functions of the LF pressure for a transmitting frequency of 10 MHz. Circles: increasing LF pressure, crosses: decreasing LF pressure.

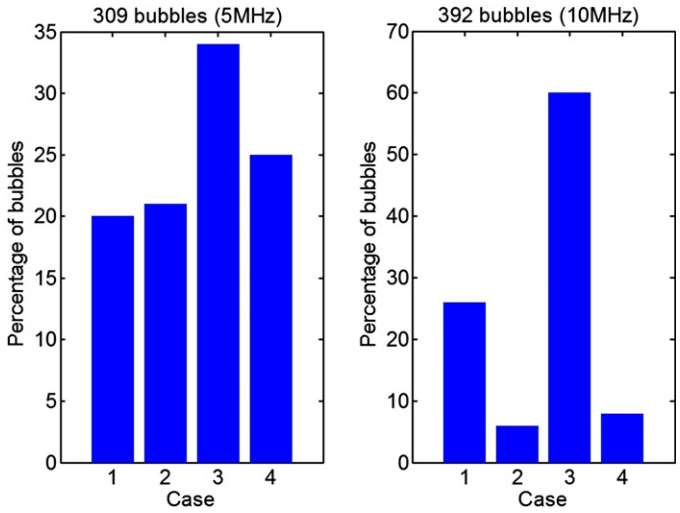

Figure 7. Prevalence of the four cases presented in figures 5 and 6 for transmitting frequencies of 5 (left panel) and 10 MHz (right panel).

Table 1. Four categories of modulation of the subharmonic and fundamental amplitudes versus the ambient pressure change.

Case 1	RFM in phase and RSM in phase
Case 2	RFM in phase and RSM out of phase
Case 3	RFM out of phase and RSM in phase
Case 4	RFM out of phase and RSM out of phase

same US signal transmitted in the experiments was applied in the simulations as the input for the bubble excitation. To mimic the effect of the LF pressure signal, which results in a change of the bubbles' initial diameter, the scattered US signal was also calculated for the same bubbles after considering $\pm 5\%$ radial strain from their equilibrium diameter. Such a radial strain is expected when applying an overpressure/depression of 15 kPa (Frinking *et al* 2010, Katiyar *et al* 2011). Then, fundamental and subharmonic scattered pressure amplitudes were extracted from the Fourier transform of the signals and RFM and RSM for each bubble size were calculated. Finally, by comparing the phase between RFM, RSM and the LF pressure, the four possible cases observed in the experiments were constructed. As an example, the fundamental and subharmonic scattered pressure amplitudes as a function of bubble diameter are presented in figure 8. These results are calculated using Marmottant *et al's* (2005) model at a transmit frequency of 10 MHz. The shell parameters needed for this model were chosen as follows: initial surface tension ($\sigma(R_0)$) at equilibrium equals 0.06 N m^{-1}, elasticity (χ) and shell viscosity (κ_s) are set to 0.4 N m^{-1} and 10^{-10} kg s^{-1}, respectively. Broken curves in figures 8(a) and (b) represent the scattered amplitudes after ambient pressure decrease (+5% radial strain, i.e. bubble expansion). Chain curves show the fundamental and subharmonic amplitudes after ambient pressure increase (-5% radial strain, i.e. bubble compression). Whenever the difference between the scattered fundamental amplitudes in compression and expansion is positive, by definition, the relative modulation is in phase with the LF pressure. If this difference is negative, the modulation is out of phase with the LF pressure. The combination of different phase behavior for RFM and RSM presents the four cases defined in experimental results. Note that the same simulations were conducted for a 5 MHz transmit frequency. They lead to the same conclusions and very similar patterns were obtained except that subharmonic emission occurs for bubble diameters ranging between 2.7 and 4.5 μm.

Numerical simulations based on the de Jong model (visco-elastic shell). The simulations were repeated using de Jong *et al's* (1994) model. This model approximates the coating of the microbubbles as a visco-elastic material. The equilibrium surface tension is equal to the surface tension between the core gas and the surrounding medium (in this case water). The other shell parameters (elasticity and viscosity) were kept the same as in the previous simulations. The outcome of the simulations predicted only cases 2 and 3 independently of the choice of shell elasticity and viscosity. This indicates that the behavior of contrast agent microbubbles observed experimentally cannot be fully explained with the de Jong *et al* model. However, the Marmottant *et al* model, taking into account buckling and rupture of the phospholipid shell, is able to predict all four cases. Note that the same simulations were conducted for a 5 MHz transmit frequency. They lead to the same conclusions and very similar patterns were obtained except that subharmonic emission occurs for bubble diameters ranging between 2.7 and 4.5 μm.

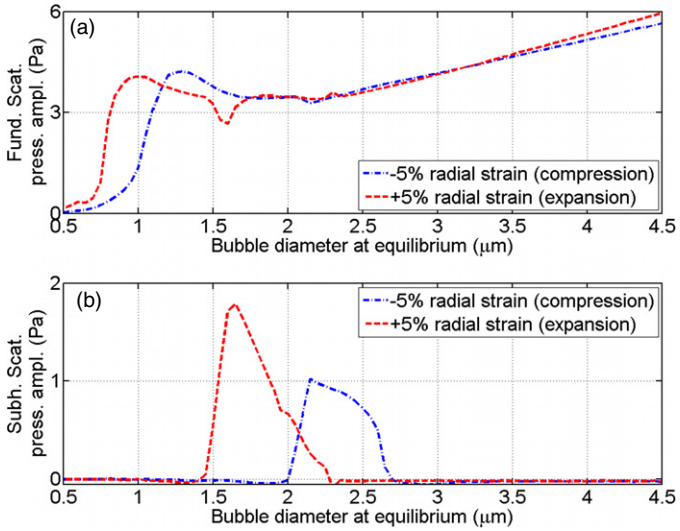

Figure 8. (a, b) Numerical computations of fundamental and subharmonic scattered pressure amplitudes (at 76 mm from the bubble) as functions of the bubble diameter based on Marmottant *et al's* (2005) model for a transmit frequency of 10 MHz. Shell parameters were set as $\sigma(R_0) = 0.06$ N m^{-1}, $\chi = 0.4$ N m^{-1} and $\kappa_s = 10^{-10}$ kg s^{-1}.

4.1.2. The influence of shell parameters on the modulation of subharmonic scattering. The determining factors in the reaction of the coated micrbubbles to a change in ambient pressure are their shell properties. It is known that among the three elastic, buckled and ruptured regimes defined for phospholipid-coated microbubbles by Marmottant *et al* (2005) depending on the initial surface tension, buckled and ruptured bubbles produce the highest subharmonic response (Sijl *et al* 2010, Faez *et al* 2011). Moreover, stiffness (or elasticity) and shell viscosity (van der Meer *et al* 2007, Faez *et al* 2011) are crucial parameters that influence the occurrence of subharmonic oscillations exhibited by phospholipid-coated bubbles. Therefore, we extended our simulations to a parametric study for a transmit frequency of 10 MHz by investigating the responses of microbubbles with diameters between 0.5 and 9 μm for initial surface tensions from 0.06 N m^{-1} to 0 N m^{-1} and shell elasticities from 2.5 to 0.25 N m^{-1}. We repeated the simulations for two different values of shell viscosity (10^{-9} and 10^{-10} kg s^{-1}) reported in the literature (van der Meer *et al* 2007, Overvelde *et al* 2010, Faez *et al* 2011). The results are shown in figures 9(a) and (b) for $\kappa_s = 10^{-9}$ and 10^{-10} kg s^{-1}, respectively.

Based on the results of simulations in figure 9, microbubbles showing cases 1 and 2 are bubbles with high initial surface tension (close to rupture) and low elasticity. Microbubbles presenting cases 3 and 4 can be either close to rupture or buckling regimes and have higher elasticity of those presenting cases 1 and 2. Moreover, the main effect of shell viscosity is on the occurrence of case 2. Decreasing the value of shell viscosity reduces the damping of the system and subsequently enhances the conditions under which case 2, and to some extent case 3, occurs.

The experimental results showed that a majority of the bubbles investigated at 10 MHz belong to cases 3 and 1 (figure 7). Simulations indicated that these bubbles should be either in (or very close to) the buckled or ruptured state. These bubbles are expected to respond asymmetrically to the change of ambient pressure because the subharmonic emission as mentioned before is much higher at these two regimes compared to the elastic state (Sijl

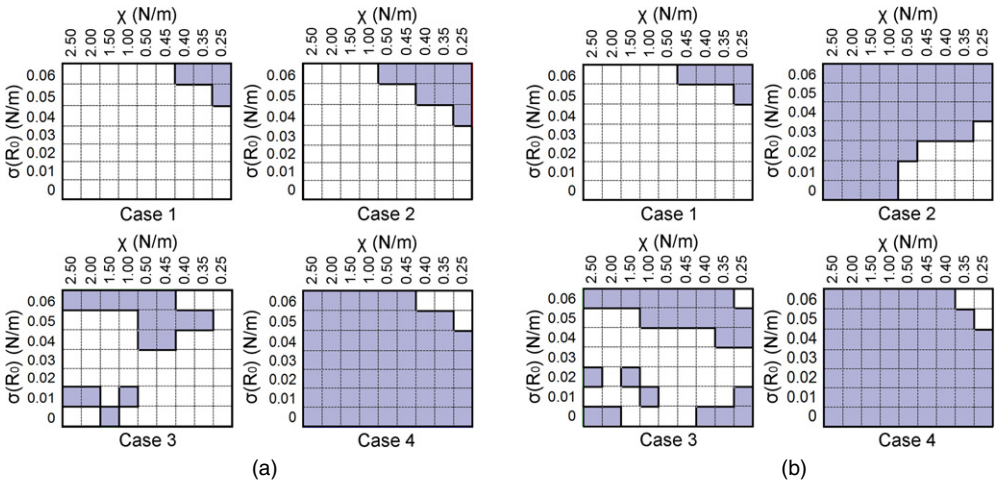

Figure 9. Occurrence of the four experimentally observed cases as functions of initial surface tension and shell elasticity of microbubbles with diameter range of 0.5–9 μm in the simulations based on Marmottant *et al's* model for (a) $\kappa_s = 10^{-9}$ kg s^{-1} and (b) $\kappa_s = 10^{-10}$ kg s^{-1}. A square is filled if the case is observed.

et al 2010, Faez *et al* 2011). This hypothesis is confirmed by the experiment (figure 6, cases 1 and 3).

4.2. Asymmetry and efficiency of subharmonic scattering modulation

A significant difference between 5 and 10 MHz transmitting frequencies is the expansion/compression asymmetry in the modulation of the subharmonic amplitude as a function of the LF pressure that occurs frequently when bubbles are insonified at 10 MHz (figure 6) but very rarely when insonified at 5 MHz (figure 5). Therefore, we performed a second-order polynomial fit on RFM and RSM versus LF pressure which provides the average curvature and the slope to obtain quantitative information about the asymmetry and the efficiency in the modulation, respectively. The slope and the curvature exhibited by the subharmonic modulation averaged for each case are displayed in figure 10. Based on figure 10, the most efficient subharmonic modulation occurs at 10 MHz for cases 1 and 3. As for the asymmetry in the modulation, for all four cases at 5 MHz there is no significant asymmetry while at 10 MHz, cases 1 and 3 indicate a substantial asymmetry.

4.3. Estimation of bulk elastic modulus

When bubbles are insonified at a transmitting frequency far above their resonance frequency, the scattered acoustic pressure is proportional to the diameter of the bubble (Maresca *et al* 2010). Therefore, by looking at the fundamental amplitude modulation of the bubbles at 10 MHz, one can estimate the relative modulation of the bubble radius. Subsequently, the bulk elastic modulus (K_v) of these bubbles can be deduced as follows (Marmottant *et al* 2005):

$$K_v = \frac{P_{\mathrm{LF}}}{\Delta V/V_0} = \frac{P_{\mathrm{LF}}}{3\Delta R/R_0} = \frac{1}{3\mathrm{RFM}_{\mathrm{slope}}}. \tag{2}$$

Here, $\mathrm{RFM}_{\mathrm{slope}}$ is the slope of the fit on the relative fundamental modulation with the LF pressure (see figure 6). For a buckled bubble, K_v is equal to κP_0 (Marmottant *et al* 2005),

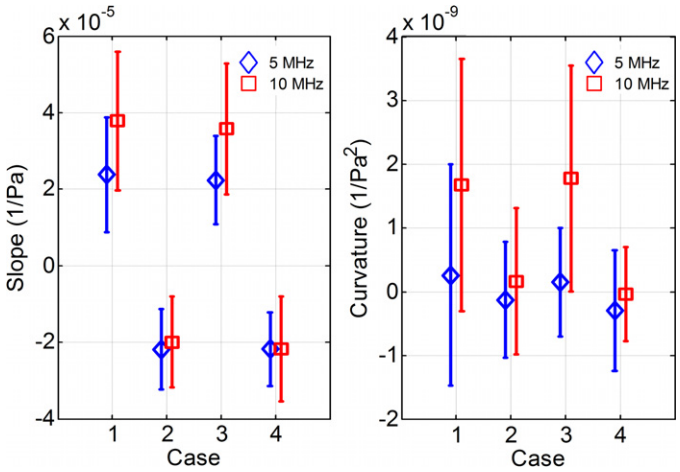

Figure 10. Subharmonic modulation efficiency (slope) and extent of the asymmetry in the subharmonic modulation (curvature) for the four cases, when bubbles are insonified at 5 (diamonds) and 10 MHz (squares).

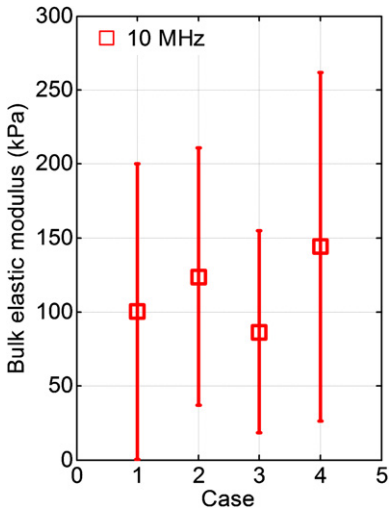

Figure 11. Bulk elastic modulus of the microbubbles deduced from RFM at 10 MHz driving frequency.

where κ is the polytropic exponent whose value is 1 for an isothermal vibration, and equals the ratio of specific heats for a bubble behaving adiabatically (1.07 for C_4F_{10}). P_0 is the ambient pressure. Figure 11 shows the bulk elastic modulus calculated from equation (2). The estimated bulk elastic modulus in four cases is around 100 kPa, i.e. the atmospheric pressure, hence in the same order of magnitude as theoretical predictions for a buckling bubble.

4.4. TR and T2R subharmonic oscillations

Two categories of subharmonic oscillations are described in the literature (Chomas *et al* 2002): transmit at resonance (TR) subharmonic and transmit at twice resonance (T2R) subharmonic. The TR subharmonic oscillations are predicted to occur when the transmit frequency is the same as the bubble resonance frequency. T2R subharmonic emission is predicted to occur when a bubble is insonified at twice its resonance frequency. The results of our simulations based on Marmottant *et al's* (2005) model are able to predict both categories of subharmonic oscillations: T2R at MI $\lesssim 0.05$ (Faez *et al* 2011) and TR at MI $\gtrsim 0.05$. However, under our experimental conditions the TR subharmonic radiation (diameter range of 1.5–2.7 μm) is always dominant, in agreement with Katiyar and Sarkar (2011). In contrast, by applying de Jong *et al's* (1994) model only T2R subharmonic contents (diameter range of 2.7–4.5 μm) are constructed (also indicated by Katiyar and Sarkar (2011)). All four cases observed in the experiments are predictable by Marmottant *et al's* (2005) model producing TR subharmonic emission only (figure 8(b)). Based on de Jong *et al's* (1994) model, only cases 2 and 3 are predicted. Therefore, it can be concluded that investigated bubbles in these experiments have mainly exhibited TR subharmonic oscillations.

4.5. Prevalence of four cases

The prevalence of the four cases derived experimentally (figure 7) indicates that for a 10 MHz transmit frequency cases 1 and 3 are dominant. Simulations predict that these cases occur within the bubble range of 2.1–2.7 μm. The size distribution of BR14 microbubbles is peaked around the diameter of 2–2.5 μm and typically looks like a chi-square function (Schneider *et al* 1997, Conversano *et al* 2010). Therefore, cases 1 and 3 result to be the most probable for a 10 MHz transmit frequency and TR subharmonic scattering.

By reducing the transmit frequency, the size range of the bubbles producing TR subharmonic scattering shifts to larger diameters. At 5 MHz, the bubble range in which the four cases occurs shifts to bubble diameters between 2.7 and 4.5 μm. Looking back to the size distribution of BR14, in this case the possibility for all four cases to occur increases, in agreement with experimental observations (figure 7).

4.6. Comparison with the literature

We report enhancement from 2 to 10 dB (in amplitude) in the subharmonic scattering of phospholipid-coated microbubbles by applying an ambient overpressure of 15 kPa. This observation is lower than the previously mentioned results of Frinking *et al* (2010). This discrepancy may arise for two reasons, presumably due to either a novel property of the experimental agent used by Frinking and colleagues or a lower acoustic pressure amplitude being employed in their experiments, 50 kPa peak negative pressure at 4 MHz (MI = 0.025). Consequently, they may have observed T2R subharmonic emission while mostly TR subharmonic was generated in our study. Besides, the possibility of manipulating the subharmonic oscillations of microbubbles in a dynamic manner makes this method suitable for imaging.

Katiyar *et al* (2011) have presented a numerical study investigating the effect of ambient pressure on the subharmonic response of contrast microbubbles. According to their simulations, the ratio of the excitation frequency (f) to the resonance frequency of the microbubbles (f_0) is the determining parameter for the subharmonic response of a bubble to either increase or decrease with ambient pressure increase. However, their criterion cannot be applied in our study because the effect of buckling and rupture has not been taken into

account in their simulations. In fact, their study applies for free gas bubbles and coated bubbles with a visco-elastic shell only. We discussed before that models with the assumption of a visco-elastic coating (de Jong *et al* 1994, Hoff *et al* 2000) can only predict two typical cases out of four experimentally observed types of behavior.

Another important factor in the occurrence of different observed behavior is the amplitude of the US burst. When this amplitude is high enough, the radial excursion can induce both buckling and rupture of the shell which amplifies the subharmonic oscillations compared to a bubble which oscillates either toward the bucking or the ruptured regimes. This was the case in our simulations based on Marmottant *et al's* (2005) model. For a bubble around the resonant diameter at 10 MHz (1.2 μm), the large bubble oscillations induce both buckling and rupture of the shell.

The results derived from this study provide the basic knowledge to apply a novel method for enhancing the subharmonic response of US contrast agents. However, using a 2.5 kHz LF wave is not realistic for *in vivo* imaging, since this frequency range is audible and may cause destruction of the eardrum for an acoustic pressure of 15 kPa peak amplitude. Instead applying a relatively higher frequency around 35 kHz may be an excellent substitution for *in vivo* applications of this method. Complementary experiments in this direction are underway.

5. Conclusion

We measured the fundamental and subharmonic scattering amplitudes of phospholipid microbubbles insonified at 5 and 10 MHz while changing the ambient pressure of the surrounding liquid in a quasi-static manner by applying a LF acoustic wave of 2.5 kHz frequency (15 kPa peak amplitude). The subharmonic amplitude was enhanced up to 10 dB by this method. Four cases were observed in the experiments and reproduced by simulations as a function of microbubbles' diameter. The prevalence of these four types of behavior is determined by the size distribution of contrast agent microbubbles.

We believe that this experimental method may be a useful tool for *in vitro* characterization and design of contrast agent microbubbles. Furthermore, this technique could be employed as a new subharmonic imaging modality.

References

Baldassarre D, Amato M, Bondioli A, Sirtori C R and Tremoli E 2000 Carotid artery intima-media thickness measured by ultrasonography in normal clinical practice correlates well with atherosclerosis risk factors *Stroke* **31** 2426–30

Brock-Fisher G A, Poland M D and Rafter P G 1996 Means for increasing sensitivity in non-linear ultrasound imaging systems *US Patent No* 5577505

Burns P N, Hope Simpson D and Averkiou M A 2000 Nonlinear imaging *Ultrasound Med. Biol.* **26** 19–22

Chomas J E, Dayton P, May D and Ferrara K 2002 Nondestructive subharmonic imaging *IEEE Trans. Ultrason. Ferroelectr. Freq. Control* **49** 883–92

Coli S, Magnoni M, Sangiorgi G, Marrocco-Trischitta M M, Melisurgo G, Mauriello A, Spagnoli L, Chiesa R, Cianflone D and Maseri A 2008 Contrast-enhanced ultrasound imaging of intraplaque neovascularization in carotid arteries: correlation with histology and plaque echogenicity *J. Am. Coll. Cardiol.* **52** 223–30

Conversano F, Franchini R and Casciaro S 2010 Characterization of microbubble contrast agents for echographic imaging through time-scheduled size distribution measurements *Sensors Transducers J.* **9** 21–7

de Jong N, Cornet R and Lancee C T 1994 Higher harmonics of vibrating gas-filled microspheres. Part one: simulations *Ultrasonics* **32** 447–53

Eliasziw M, Rankin R N, Fox A J, Haynes R B and Barnett H J M 1995 Accuracy and prognostic consequences of ultrasonography in identifying severe carotid artery stenosis *Stroke* **26** 1747–52

Faez T, Emmer M, Docter M, Sijl J, Versluis M and de Jong A 2011 Characterizing the subharmonic response of phospholipid-coated microbubbles for carotid imaging *Ultrasound Med. Biol.* **37** 958–70

Feinstein S B 2006 Atherosclerotic plaque neovascularization contrast ultrasound imaging of the carotid artery vasa vasorum and atherosclerotic plaque neovascularization *J. Am. Coll. Cardiol.* **48** 236-243

Forsberg F, Piccoli C W, Merton D A, Palazzo J J and Hall A L 2007 Breast lesions: imaging with contrast-enhanced subharmonic US—initial experience *Radiology* **244** 718–26

Frinking P J A, Gaud E, Brochot J and Arditi M 2010 Subharmonic scattering of phospholipid-shell microbubbles at low acoustic pressure amplitudes *IEEE Trans. Ultrason. Ferroelectr. Freq. Control* **57** 1762–71

Goertz D E, Frijlink M E, Tempel D, Bhagwandas V, Gisolf A, Krams R, de Jong N and van der Steen A F W 2007 Subharmonic contrast intravascular ultrasound for vasa vasorum imaging *Ultrasound Med. Biol.* **33** 1859–72

Goertz D E, Needles A, Burns P N and Foster F S 2005 High-frequency, nonlinear flow imaging of microbubble contrast agents *IEEE Trans. Ultrason. Ferroelectr. Freq. Control* **52** 495–502

Hoff L, Sontum P C and Hovem J M 2000 Oscillations of polymeric microbubbles: effect of the encapsulating shell *J. Acoust. Soc. Am.* **107** 2272–80

Katiyar A and Sarkar K 2011 Excitation thresholds for subharmonic response of ultrasound contrast microbubbles *POMA* **11** 020003

Katiyar A, Sarkar K and Forsberg F 2011 Modeling subharmonic response from contrast microbubbles as a function of ambient static pressure *J. Acoust. Soc. Am.* **129** 2325–35

Maresca D, Emmer M, Van Neer P, Vos H J, Versluis M, Muller M, de Jong N and Van der Steen A F 2010 Acoustic sizing of an ultrasound contrast agent *Ultrasound Med. Biol.* **36** 1713–21

Marmottant P, van der Meer S, Emmer M, Versluis M, de Jong N, Hilgenfeldt S and Lohse D 2005 A model for large amplitude oscillations of coated bubbles accounting for buckling and rupture *J. Acoust. Soc. Am.* **118** 3499–505

Needles A, Arditi M, Rognin N G, Mehi J, Coulthard T, Bilan-Tracey C, Gaud E, Frinking P, Hirson D and Foster F S 2010 Nonlinear contrast imaging with an array based micro-ultrasound system *Ultrasound Med. Biol.* **36** 2097–106

Overvelde M, Garbin V, Sijl J, Dollet B, de Jong N, Lohse D and Versluis M 2010 Nonlinear shell behavior of phospholipid-coated microbubbles *Ultrasound Med. Biol.* **36** 2080–92

Renaud G, Calle S and Defontaine M 2009 Remote dynamic acoustoelastic testing: elastic and dissipative acoustic nonlinearities measured under hydrostatic tension and compression *Appl. Phys. Lett.* **94** 011905-3

Renaud G, Calle S and Defontaine M 2010 Dynamic acoustoelastic testing of weakly pre-loaded unconsolidated water-saturated glass beads *J. Acoust. Soc. Am.* **128** 3344–54

Renaud G, Calle S, Remenieras J P and Defontaine M 2008 Exploration of trabecular bone nonlinear elasticity using time-of-flight modulation *IEEE Trans. Ultrason. Ferroelectr. Freq. Control* **55** 1497–507

Schneider M, Broillet A, Bussat P, Giessinger N, Puginier J, Ventrone R and Yan F 1997 Gray-scale liver enhancement in VX2 tumor-bearing rabbits using BR14, a new ultrasonographic contrast agent *Investigative Radiol.* **32** 410–7

Shah F, Balan P, Weinberg M, Reddy V, Neems R, Feinstein M, Dainauskas J, Meyer P, Goldin M and Feinstein S B 2007 Contrast-enhanced ultrasound imaging of atherosclerotic carotid plaque neovascularization: a new surrogate marker of atherosclerosis? *Vasc. Med.* **12** 291–7

Shalhoub J, Owen D R J, Gauthier T, Monaco C, Leen E L S and Davies A H 2010 The use of contrast enhanced ultrasound in carotid arterial disease *Eur. J. Vasc. Endovasc. Surg.* **39** 381–7

Shi W T, Forsberg F, Hall A L, Chiao R Y, Liu J B, Miller S, Thomenius K E, Wheatley M A and Goldberg B B 1999 Subharmonic imaging with microbubble contrast agents: initial results *Ultrason. Imaging* **21** 79–94

Sijl J, Dollet B, Overvelde M, Garbin V, Rozendal T, de Jong N, Lohse D and Versluis M 2010 Subharmonic behavior of phospholipid-coated ultrasound contrast agent microbubbles *J. Acoust. Soc. Am.* **128** 3239–52

Staub D, Patel M B, Tibrewala A, Ludden D, Johnson M, Espinosa P, Coll B, Jaeger K A and Feinstein S B 2009 Vasa vasorum and plaque neovascularization on contrast-enhanced carotid ultrasound imaging correlates with cardiovascular disease and past cardiovascular events *Stroke* **41** 41–7

Tang M X, Kamiyama N and Eckersley R J 2010 Effects of nonlinear propagation in ultrasound contrast agent imaging *Ultrasound Med. Biol.* **36** 459–66

van der Meer S M, Dollet B, Voormolen M M, Chin C T, Bouakaz A, de Jong N, Versluis M and Lohse D 2007 Microbubble spectroscopy of ultrasound contrast agents *J. Acoust. Soc. Am.* **121** 648–56

Vicenzini E, Giannoni M F, Puccinelli F, Ricciardi M C, Altieri M, Di Piero V, Gossetti B, Benedetti Valentini F and Lenzi G L 2007 Detection of carotid adventitial vasa vasorum and plaque vascularization with ultrasound cadence contrast pulse sequencing technique and echo-contrast agent *Stroke* **38** 2841–3

Xiong L, Deng Y B, Zhu Y, Liu Y N and Bi X J 2009 Correlation of carotid plaque neovascularization detected by using contrast-enhanced US with clinical symptoms *Radiology* **251** 583–9